Received December 5, 2014, accepted March 5, 2015, date of publication July 17, 2015, date of current version August 11, 2015.

Digital Object Identifier 10.1109/ACCESS.2015.2454533

Making Bertha See Even More: Radar Contribution

JUERGEN DICKMANN, NILS APPENRODT, JENS KLAPPSTEIN, HANS-LUDWIG BLOECHER, MARC MUNTZINGER, ALFONS SAILER, MARKUS HAHN, AND CARSTEN BRENK

Daimler AG, Ulm 89081, Germany

Corresponding author: N. Appenrodt (nils.appenrodt@daimler.com)

ABSTRACT For decades, radar has been applied extensively in warfare, earth observation, rain detection, and industrial applications. All those areas are characterized by requirements such as high quality of service, reliability, robustness in harsh environment and short update time for environmental perception, and even imaging tasks. In the vehicle safety and driver assistance field, radars have found widespread application globally in nearly all vehicle brands. With the market introduction of the 2014 Mercedes-Benz S-Class vehicle equipped with six radar sensors covering the vehicles environment 360° in the near (up to 40 m) and far range (up to 200 m), autonomous driving has become a reality even in low-speed highway scenarios. A large azimuth field of view, multimodality and a high update rate have been the key innovations on the radar side. One major step toward autonomous driving was made in August 2013. A Mercedes-Benz research S-Class vehicle—referred to at Mercedes as Bertha—drove completely autonomously for about 100 km from Mannheim to Pforzheim, Germany. It followed the well-known historic Bertha Benz Memorial Route. This was done on the basis of one stereo vision system, comprising several long and short range radar sensors. These radars have been modified in Doppler resolution and dramatically improved in their perception capabilities. The new algorithms consider that urban scenarios are characterized by significantly shorter reaction and observation times, shorter mean free distances, a 360° interaction zone, and a large variety of object types to be considered. This paper describes the main challenges that Daimler radar researchers faced and their solutions to make Bertha see.

INDEX TERMS Radar, automotive radar, autonomous driving.

I. INTRODUCTION

In themselves, autonomously moving cars are nothing new. From 2004 to 2007 DARPA initiated the Grand and Urban Challenge competition for autonomous driving in landscape areas [4]. The vehicles were equipped with a huge number of widely varying sensors. Today BMW prototypes drive on the highway between Munich and Nuremberg, Google cruises with their robot car through Nevada and California. Recently Audi demonstrated a driverless ride in a multi-story car park in Las Vegas. However, the technical equipment was far from standard.

In 2014 a brand-new Mercedes-Benz S-Class named ''Bertha'' drove the Bertha Benz Memorial Route in a fully autonomous manner, see Figure 1. In August 1888, Bertha Benz used her husband Carl Benz's three-wheeled vehicle to drive from Mannheim to Pforzheim, Germany. This historic event is nowadays looked upon as the birth date of the modern automobile. Following the official Bertha Benz Memorial Route, the S-Class drove through downtown Heidelberg, passed by the Bruchsal Castle, and through narrow villages in the Black Forest. It made its way through numerous intersections and roundabouts, planned its path through narrow passages with oncoming vehicles and numerous cars parked on the road, and gave the right of way to crossing pedestrians. While Bertha Benz wanted to demonstrate the maturity of the gasoline engine developed by her husband, the goal of the present experiment was to show that autonomous driving is possible on highways, similar well-structured environments, and inner city roads, using near serial-production sensor equipment. An additional aim was to identify further research directions for all fields of action such as radars and radar-based perception. Standard-production sensor set-ups are enhanced by adding radars with a drastically higher Doppler resolution to cover critical situations like roundabouts and crossings, as shown in Fig. 2. The main differences compared to the serial radars are special

FIGURE 1. Autonomous vehicle "Bertha", a 2014 Mercedes- Benz S-Class with well-integrated close-to-production sensors driving fully autonomously on open public roads.

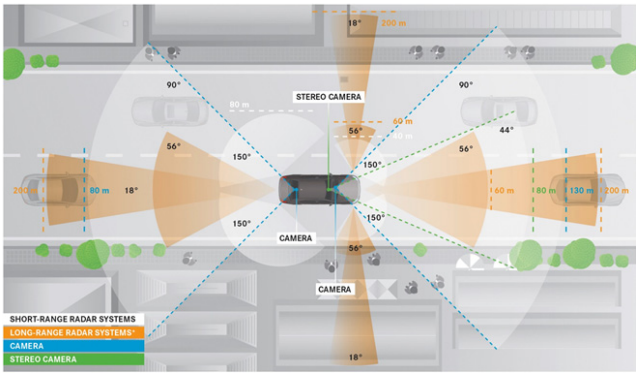

FIGURE 2. Sensor set-up of autonomous vehicle "Bertha". One stereo-vision system looking forward and one mono system for backward. Eight radar sensors covering 360° up to 200m.

algorithms developed for environmental representation tasks based on the radar's measurement data.

This was necessary since compared to standard highway scenarios, urban scenarios are characterized by dramatic differences in situations which a radar sensor has to handle. In detail these are shorter reaction and observation times due to shorter mean-free distances between one's car and other traffic participants or obstacles. Another difference is that a 360° interaction zone has to be monitored, for which new radar-radar fusion concepts have to be developed. A large variety of different object types have to be taken into consideration. Not only detection of pedestrians is necessary, but also their classification in order to provide confidence measures. Driving lane detection and prediction on highways and rural roads is mandatory for autonomous driving and maneuvering. The support in adverse light and weather conditions has to be warranted by the radar system. For this task, new algorithm concepts also have to be developed. Clustering and tracking of distributed objects will become more important in order to assess and predict scenarios appropriately in roundabouts and crossing situations. Up to the Bertha drive, dealing with stationary environment in addition to dynamic objects was not an issue. For autonomous driving it is an essential add-on and has to be solved. Hence, the environmental perception tasks the Bertha radar set-up has to perform in urban and rural scenarios goes far beyond that of present day ACC or Pre-Safe emergency braking tasks.

For the radar sensor, this translates into questions about the optimum frequency of operation and the appropriate bandwidth. In parallel to algorithm development, regulatory issues have to be addressed. Finally, the challenges on packaging issues for vehicle integration have to be solved.

The preparations for Bertha's drive initiated the metamorphosis of the radar from a simple detector to an imaging like device: A radar-eye.

The following chapters present the solutions which let Bertha see.

II. RADAR ARCHITECTURE AND FUSION FOR 360° COVERAGE AND PERCEPTION

The Radar sensors set-up for realizing the complete 360 degree coverage in day and night is shown in Figure 2. As will be described in detail in Section VII, one main advantage of radar technology is the invisible packaging of the sensors behind the bumpers. This fact was taken in consideration when designing the radar architecture with reference to the large field of view (FoV) provided from each single sensor of over 140 degree. As can be seen in Figure 2, the FoV of the radars overlap partly, which provides higher sensor redundancy in important regions and allows for easier sensor fusion. Hence, with only four sensors at each corner of the vehicle, it is possible to provide a 360 degree global object list via an intelligent sensor data fusion.

The overview of the multi-sensor multi-target tracking system is schematically illustrated in Figure 3. The sensor technology module obtains information on the vehicle's environment. This information is then processed using various signal processing algorithms. The results are forwarded to the application layer. The main focus of this section will be the signal processing module.

Sensor fusion techniques have the inherent problem of measurements from different radar sensors arriving at the processing unit out-of-sequence, i.e., the original temporal ordering of measurements is lost. This problem is known in literature as the out-of-sequence-measurement problem [5].

Usually this problem is solved via buffering all incoming measurements to ensure the correct temporal order. However, for autonomous driving applications, where the driver is not in the loop anymore, temporal delays caused by the sensor fusion have to be avoided by all means [6]. Through the advanced out-of-sequence algorithms, the state estimation is more accurate and increases the overall system performance of autonomous driving applications.

Figure 4 illustrates an example of an out-of-sequence measurement problem. In this example, measurements from sensor 2 have a shorter latency and arrive earlier than sensor 1 at the fusion level. The measurements from sensor 1 have a different updated rate and a larger latency than sensor 2.

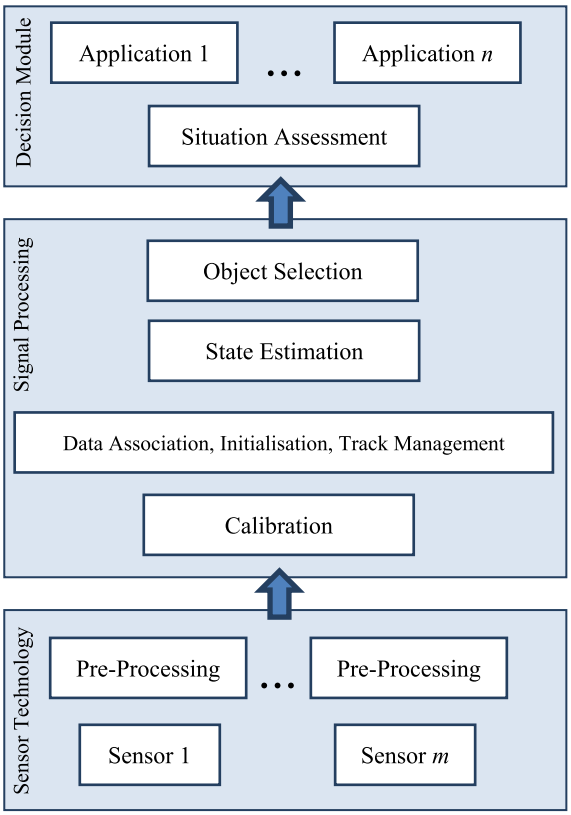

FIGURE 3. Data flow of a multi-target multi-sensor tracking system.

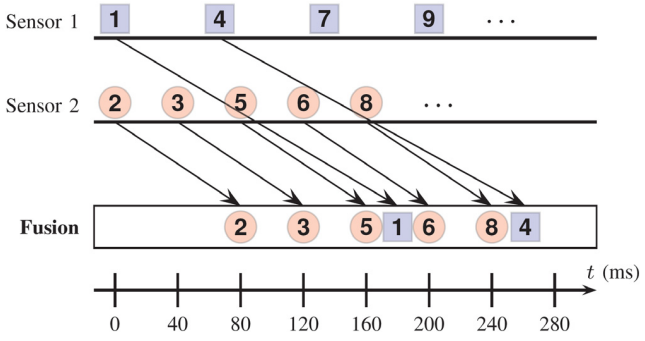

FIGURE 4. Out-of-sequence measurement problem.

Therefore, the measurements from sensor 2 will always arrive out-of-sequence with respect to the time of the last measurement update by the Kalman filter.

The example illustrated in Figure 4 shows an l-lag problem, where l represents the number of time steps behind the current track time [7]. The l-lag problem can be reduced to a 1-lag problem by calculating an equivalent measurement as follows [6]:

$$
\begin{aligned}
\mathrm{R}_{\mathrm{k}}^{*-1} &= \mathrm{P}_{\mathrm{k|k}}^{-1} - \mathrm{P}_{\mathrm{k|k-1}}^{-1} \\
\mathrm{K}_{\mathrm{k}}^{*} &= \mathrm{P}_{\mathrm{k|k}} \mathrm{R}_{\mathrm{k}}^{*-1} \\
\gamma_{\mathrm{k}}^{*} &= \mathrm{K}_{\mathrm{k}}^{*-1} \left[\mathrm{x}_{\mathrm{k|k}} - \mathrm{x}_{\mathrm{k|k-1}} \right] \\
\mathrm{S}_{\mathrm{k}}^{*-1} &= \mathrm{P}_{\mathrm{k|k-1}}^{-1} - \mathrm{P}_{\mathrm{k|k-1}}^{-1} \left[\mathrm{P}_{\mathrm{k|k-1}}^{-1} + \mathrm{R}_{\mathrm{k}}^{*-1} \right]^{-1} \mathrm{P}_{\mathrm{k|k-1}}^{-1}
\end{aligned}
$$

The purpose for the equivalent measurement is to adapt the l-lag-problem to a 1-lag problem by combining all the measurement between time step k-l and k into the so called equivalent measurement. After having calculated the equivalent measurement $\mathrm{R}_{\mathrm{k}}^{*}$ and the equivalent Kalman gain $\mathrm{K}_{\mathrm{k}}^{*}$, the state and covariance can be retrodicted to the out-of-sequence-measurement time k_0 by

$$
\begin{aligned}
\mathrm{x}_{\mathrm{k_0|k}} &= \mathrm{F}_{\mathrm{k_0|k}} \left[\mathrm{x}_{\mathrm{k|k}} - \mathrm{Q}_{\mathrm{k|k_0}} \mathrm{S}_{\mathrm{k}}^{*-1} \gamma_{\mathrm{k}}^{*} \right] \\
\mathrm{P}_{\mathrm{k,k_0|k}}^{\mathrm{vv}} &= \mathrm{Q}_{\mathrm{k|k_0}} - \mathrm{Q}_{\mathrm{k|k_0}} \mathrm{S}_{\mathrm{k}}^{*-1} \mathrm{Q}_{\mathrm{k|k_0}} \\
\mathrm{P}_{\mathrm{k,k_0|k}}^{\mathrm{xv}} &= \mathrm{Q}_{\mathrm{k|k_0}} - \mathrm{P}_{\mathrm{k|k-1}} \mathrm{S}_{\mathrm{k}}^{*-1} \mathrm{Q}_{\mathrm{k|k_0}} \\
\mathrm{P}_{\mathrm{k_0|k}} &= \mathrm{F}_{\mathrm{k_0|k}} \left[\mathrm{P}_{\mathrm{k|k}} + \mathrm{P}_{\mathrm{k,k_0|k}}^{\mathrm{vv}} - \mathrm{P}_{\mathrm{k,k_0|k}}^{\mathrm{xv}} - \left(\mathrm{P}_{\mathrm{k,k_0|k}}^{\mathrm{xv}} \right)^{\mathrm{T}} \right] \mathrm{F}_{\mathrm{k_0|k}}^{\mathrm{T}}
\end{aligned}
$$

The covariance matrix $\mathrm{Q}_{\mathrm{k|k_0}}$ describes the process noise in the interval $[k, k_0]$. At this point, the out-of-sequence measurement $\mathrm{z}_{\mathrm{k_0}}$ can be directly integrated as follows

$$
\begin{aligned}
\mathrm{S}_{\mathrm{k_0}} &= \mathrm{H}_{\mathrm{k_0}} \mathrm{P}_{\mathrm{k_0|k}} \mathrm{H}_{\mathrm{k_0}}^{\mathrm{T}} + \mathrm{R}_{\mathrm{k_0}} \\
\mathrm{P}_{\mathrm{k,k_0|k}}^{\mathrm{xz}} &= \left[\mathrm{P}_{\mathrm{k|k}} - \mathrm{P}_{\mathrm{k,k_0|k}}^{\mathrm{xv}} \right] \mathrm{F}_{\mathrm{k_0|k}}^{\mathrm{T}} \mathrm{H}_{\mathrm{k_0}}^{\mathrm{T}} \\
\mathrm{W}_{\mathrm{k_0}} &= \mathrm{P}_{\mathrm{k,k_0|k}}^{\mathrm{xz}} \mathrm{S}_{\mathrm{k_0}}^{-1} \\
\mathrm{x}_{\mathrm{k|k_0}} &= \mathrm{x}_{\mathrm{k|k}} + \mathrm{W}_{\mathrm{k_0}} \left[\mathrm{z}_{\mathrm{k_0}} - \mathrm{H}_{\mathrm{k_0}} \mathrm{x}_{\mathrm{k_0|k}} \right] \\
\mathrm{P}_{\mathrm{k|k_0}} &= \mathrm{P}_{\mathrm{k|k}} - \mathrm{P}_{\mathrm{k,k_0|k}}^{\mathrm{xz}} \mathrm{S}_{\mathrm{k_0}}^{-1} (\mathrm{P}_{\mathrm{k,k_0|k}}^{\mathrm{xz}})^{\mathrm{T}}
\end{aligned}
$$

where $\mathrm{x}_{\mathrm{k|k_0}}$ and $\mathrm{P}_{\mathrm{k|k_0}}$ are the new state and the new covariance at time k with the out-of-sequence measurement integrated.

The main advantage of using advanced out-of-sequence measurements algorithms is the computational benefit, while having the same tracking performance as reprocessing all measurements at the out-of-sequence time. In an autonomous driving application, where computers have control over the vehicle, temporal delays caused by the sensor fusion have to be avoided by all means.

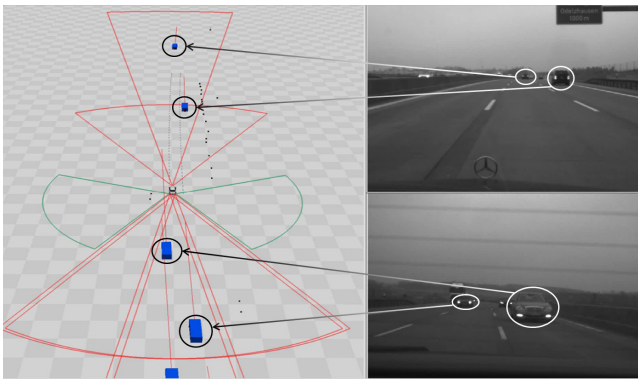

FIGURE 5. In-vehicle interface of the signal processing result. The blue boxes represent classified tracked objects.

The resulting 360 degree tracking is shown in Figure 5. The blue boxes represent the moving tracked objects that are forwarded to the situation assessment module. This description of the ego-vehicle environment can be utilized for instance to process the decision to initiate an autonomous lane

change maneuver. It is vital to quickly and accurately estimate the *pose,* i.e. position and orientation, in the area around the vehicle. To improve the estimation, several radar sensors are fused to one global track management. In case the field of view does not cover the entire 360 degree, a model based approach need to be considered.

The rear traffic needs to be observed for a lane change application. The tracking system must especially intervene a lane change request if fast vehicles approaches from behind.

Furthermore, it is crucial to achieve a continuous tracking of all objects around the car. In doing so, the most challenging part is the data association of a point target to a two-dimensional object. The objects are described by the pose, the width and the length. The raw targets are clustered and the resulting reference target is integrated into the state estimation of the Kalman filter.

Altogether, for autonomous driving applications it is important to process an out-of-sequence measurement with advanced algorithms in order to achieve the best system performance and to guarantee real-time capabilities.

Tracking and track management as described above is well suited to cover highway situations. Constraints on the motion of vehicles and trucks on highways can simplify tracking and fusion of objects. For instance, the tracking algorithms assume that the object motion is in one unique direction within a certain velocity range. Furthermore, the environment perception for lane change applications does not require oncoming traffic and stationary objects.

The information required for rural roads and more pronounced for urban regions requires much more ''imaging like'' information and more sophisticated object representation. The objects that are needed in inner-city traffic scenarios are not only represented by position information, but also by their dimension. The estimation of the size of the tracked objects is crucial, especially in narrows streets.

Due to our project aim to use commercially available sensors which are similar to serial production radars, some compromises had to be made. The solutions for roundabout traffic and crossroads will be described in the following section.

III. ROUNDABOUT AND CROSSING SURVEILLANCE

One cluster of traffic situations which needed add on solutions to that described in Chapter II was the surveillance of crossings and roundabouts that had to be passed by Bertha during the autonomous drive. Rural roads, small villages and inner city traffic lead to a representative sample of situations that the radar platform had to cope with. For example, not less than 18 different roundabouts are located on the Bertha Benz route. The following sections will give an overview about the processing framework without the claim to reveal all details of the underlying algorithms.

For a safe decision that the autonomous vehicle could proceed on the pre-defined route, the sensor platform had to ensure that no other traffic participant was crossing the vehicle path or the roundabout was not occupied by other vehicles. Solving this problem means providing a robust monitoring of the frontal and side region of the vehicle which is able to detect all moving objects up to the field of view range of the individual sensors. Crossing situations on rural road junctions with fast moving vehicles up to 70 kph was the root cause for implementing the two side long-range radar sensors on the front end of the vehicle. A special derivative of long range radar that is already used in Mercedes series production cars for some years was chosen to solve this task. Major parameters of this radar are noted in Table 1. An advantage of this solution is that it is possible to access different data processing levels of the sensor to obtain optimal use of the sensor performance. As depicted in Figure 2, the long range radar senses a broader mid-range region beside the narrow long range field of view.

TABLE 1. Sensor parameters of the long range radars for crossing surveillance and rear monitoring.

Parameters	Far field beam	Near field beam
Range	200m	60m
Range resolution	2m	2m
Field of view	+/- 8,5°	+/- 28°
Angular resolution	1°	4°
Velocity	-73 to 24 m/s	-73 to 24 m/s
Velocity resolution	0,77 m/s	1,54 m/s
Cycle time	66 ms	66 ms

Roundabouts of different topology and inner-city crossings furthermore require gap-less monitoring of the frontal and frontal-side region. Two short-range radar sensors with a very broad field of view of 150° each were chosen to fulfil this requirement. Table 2 depicts the main radar parameters of the short range sensors. A reasonable overlap of the two radars sensing regions leads to the possibility of special signal processing and an enhanced monitoring robustness of the platform. The short-range radar sensors used allowed access to the detection level data, a pre-requisite for establishing a separate signal processing framework including stationary

TABLE 2. Sensor parameters of the short range radars for vehicle surrounding perception.

Parameters	Front radars	Rear radars
Range	40m	80m
Range resolution	0,6m	1,2m
Field of view	+/- 75°	+/- 75°
Angular resolution	n.a.	n.a.
Velocity	-55 to 15 m/s	-55 to 15 m/s
Velocity resolution	0,25 m/s	0,25 m/s
Cycle time	50 ms	50 ms

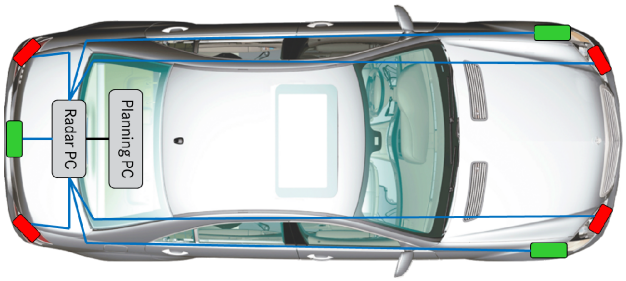

FIGURE 6. Main radar platform components overview depicting the mounting position of long range radars (green) and short range radars (red) and the private CAN connections to the radar PC.

and moving multi-object detection and tracking with classification of pedestrians (see details in Chapter IV).

The entire radar sensor network signal processing and data recording is performed on a dedicated compact PCI slot card computer board. Seven radar sensors, up to four video cameras for documentation purposes, the vehicle bus system and the planning component are connected to the radar PC. Figure 6 gives an overview over the radar platform main components and connections. The Automotive Data and Time-Triggered Framework (ADTF) running on a Linux operating system serves as a framework for the developed signal processing. The realized platform allowed the complete event-based recording of all input data streams and enabled a scenario re-processing during the development phase of the project on workstations in the lab.

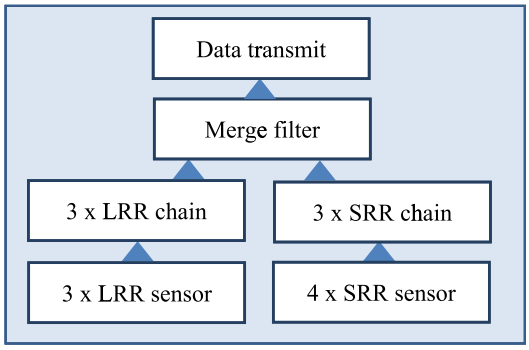

FIGURE 7. Top level system architecture overview illustrating the 6 parallel running signal processing chains based on the sensor data of 3 long range radars (LRR) and 4 short range radars (SRR). All components are supervised by the merge filter component.

Due to the stringent requirements related to fail-safe operation of each component of an autonomously driving vehicle, several measures were implemented inside the radar platform for a complete supervision of all radar system components starting from the individual radar sensors up to the components of the signal processing chain. Fast periodical radar platform status messages permitted an external failure monitoring even in case of a complete system breakdown. The radar processing was split into several parallel signal processing paths which were combined in a merging filter which collected all the processed objects from different sensors or observation regions. Figure 7 gives a first overview over the high level system architecture. Within the merging filter, the main internal system supervision was implemented. During the processing cycle inputs from the different chains are fused together and composed to the object list that represents the environment description delivered by the radar PC. The object list is then transferred to the PC hosting the object fusion and motion planning algorithms via an Ethernet connection with a cycle time of 66 milliseconds. The object description contains information about the position, motion states, spatial dimension and quality criteria.

The long range radars were integrated behind the vehicle bumpers like every other additional radar sensor. A key factor was thus the proper integration, positioning and alignment of the sensors inside the vehicle to guarantee the maximum possible range coverage. More details regarding this effort can be found in Chapter VII of this article. The long range radar sensors at the side and the backward-looking sensor are all processed individually as single sensor systems. An additional object management and state prediction algorithm was implemented that operates on the already tracked object data transmitted by the radar sensors. Rare intermediate object losses in some complex traffic situations can be prevented with this measure and continuous tracks of moving vehicles up to the maximum operation distance can be established. Furthermore, tracks that are labeled as stationary on the radar output interface or irrelevant moving objects (e.g. leaving objects on the adjacent lane that have passed the ego vehicle) are suppressed by the processing to limit the number of tracks and therefore reduce the computational load of the radar PC. The remaining tracked objects of moving traffic participants are then passed into the merge filter component.

Four short range radar sensors were integrated in the front and rear bumpers near the vehicle corners. The resulting observation coverage with only small blind spot areas at the car side vicinity is indicated in Figure 2. Three parallel running processing chains were developed to fulfil the previously discussed requirements in an optimized manner. Two of the paths combine the two frontal near range sensors and therefore cover the whole perception of the environment in the driving direction, including the frontal side region. This was necessary because the task of pedestrian detection and classification has significantly divergent requirements compared to the universal object detection and tracking sub-module. More details regarding the pedestrian processing can be found in Chapter IV.

Most of the developed algorithm components are not used in only one of the short range radar processing chains, but input signals and parameterization differ to an extent that a combination does not make sense. In the following, the processing chain of the universal object detection and tracking will be described in some more detail. Fig. 8 depicts the general algorithm architecture of the three short range radar processing chains.

As first step, many pre-processing filters have to be applied to the targets received from each individual sensor. Multiple turnaround filtering, suspicious target rejection, clutter and

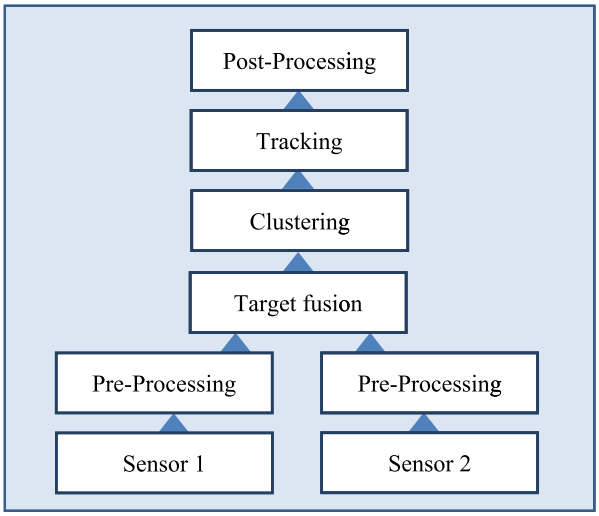

FIGURE 8. General architecture of the short range radar processing chains.

ghost target suppression is only a selection of the necessary treatment to optimize the achievable performance of the overall perception system. Two more special algorithms should be mentioned as part of the pre-processing stage. One of them implements a movement classification on the target level. The algorithm groups the targets into the static and dynamic world representation that can then be fed into different algorithm branches. The other filter is capable of identifying and rejecting targets as reflections of the ego vehicle in mirror structures like signs at the road border or guard rails. Because the short-range radar fields of views overlap in portions of the environment, sensor targets are fused together for the frontal and the rear region separately before applying further processing steps. Based on these sensor targets, cloud-extended objects are extracted from the data by using a cluster algorithm. DBSCAN [8] was implemented due to the requirement to extract objects independently from the knowledge of the number of existing targets in the current scenario. The parameterization was chosen so that a separation of different physical objects is realized in most practical scenarios. Moreover, clusters above a certain extension threshold are further analyzed to identify velocity gradients for false target suppression and calculate spatial extension measures. A set of representation points is derived from each cluster as input for the tracker stage.

Implementing a set of different Kalman trackers as a tracking framework allowed the flexible development of the multi-object tracking of spatial distributed objects. Components such as input conversion, data association, Kalman filter, and track management could be selected from an algorithm library. More details about the tracking module are given in Chapter II. The tracked objects from the frontal and rear region are then transferred to the merging filter for preparation of the comprehensive radar object list.

The developed radar sensor platform was well suited for the traffic crossing surveillance task. Inner-city crossing scenarios benefit from the 40 meter short range radar cocoon in combination with the 60 m mid-range coverage of the side long range radar sensors. For the crossways on rural roads, the fixed alignment of the relatively narrow far range field of view was a limiting factor that could be mitigated by predictive path planning for the autonomous driving vehicle. Detection and tracking of oncoming vehicles could be realized up to a distance of 200m. Figure 9 exemplarily depicts a crossing scenario to give an impression of the radar platform output data in such situation.

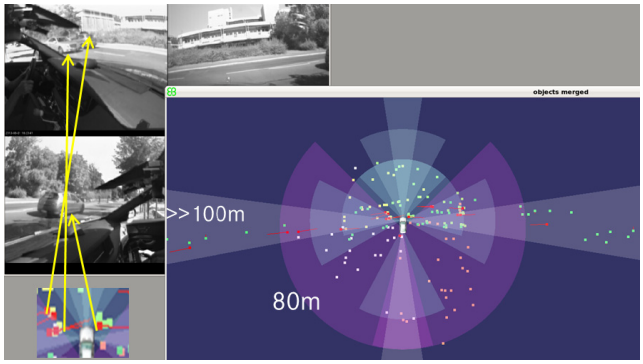

FIGURE 9. Crossing scenario illustrating the radar target data (colored points) and tracked objects (red points with line) recorded at an inner-city road junction.

The roundabout observation was solely based on the processing of the two frontal near range radar sensors. Moving objects like cars, trucks, motor cycles and bicycles could be detected and tracked early enough to enable a robust decision of the situation interpretation stage if the roundabout could be entered by the ego vehicle.

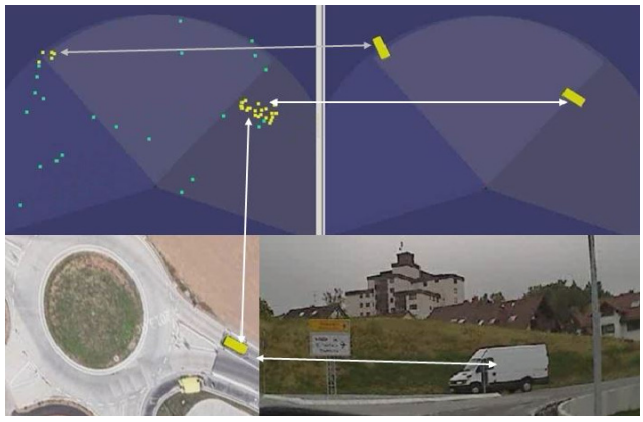

FIGURE 10. Upper left: Sensor data of the roundabout scenario with stationary (green) and moving (yellow) labeled targets; upper right: processed moving objects (yellow); lower left: map cutout of the scenario; lower right: video images of the scene from a camera looking on the right frontal side.

In Figure 10 an example of a roundabout situation is illustrated for which the wide field of view coverage of the radar platform is a necessary prerequisite. Nevertheless, especially roundabout situations turned out to be an ambitious

challenge for the radar based sensing system. Vast varieties of the roundabout topology and infrastructure were a source for a lot of surprises and future improvement measures.

IV. SIGNAL PROCESSING FOR DETECTION AND CLASSIFICATION OF PEDESTRIANS

In order to enable an autonomous car like ''Bertha'' to also drive accident free through inner-city scenarios it is mandatory not only to recognize all cars and obstacles but also all other kinds of traffic participants such as pedestrians. However, with radars, pedestrians cannot be recognized like any other object, they represent a special category of traffic participant which needs to be identified. The reason is that an autonomous car needs a special reaction after determined whether the object is a pedestrian or not.

This type of identification is called object classification. On the one hand it improves the safety for vulnerable road users and on the other hand it enables the autonomous car to interact in inner-city scenarios in an appropriate way with pedestrians, e.g., at crosswalks where Bertha needs to react early on and human-like to pedestrians heading towards the crosswalk. In such situations the car has to give the pedestrian the right of way and start decelerating early enough. It has to behave not like a safety system with a late emergency braking, but like a human driver, which means that the pedestrian feels that the car has recognized him and that he or she can pass. This interaction took place at all crosswalks along the whole historical route from Ladenburg to Pforzheim. One crosswalk on this route is of special interest, in Bruchsal near the old historical castle (see Figure 11). This crosswalk is directly after a right-turn, so that the car needs to recognize the pedestrian not only straight ahead but also far enough on both sides even behind the right turn of the street. If the car comes closer to the right-turn, the pedestrians leave the field-of-view of normal pedestrian classification sensors like cameras. The solution of this problem is only feasible with

FIGURE 11. Challenging crosswalk behind right-turn at Bruchsal.

sensors which have a wide field-of-view. The two short-range radar sensors used in the front of the car had a very broad field of view of 150° (see previous chapter) so that the complete area of interest around the front of the car and frontal side region could be covered up to a distance of 40m.

In addition to the coverage area, the pedestrian detection and classification put some other challenges on the radar sensors. Firstly, the sensors need to be very sensitive because of the weak radar reflection of pedestrians compared to cars or other metal objects. Secondly, the high sensitivity requires a high number of parallel computed radar raw detections which can be computed in every cycle. Determination from any clutter is enabled by a high signal-to-noise ratio. Thirdly, the radar sensors require very high Doppler separation ability. This last attribute enables the sensors to see multiple raw targets from the same walking pedestrian with different Doppler velocities. This so called ''Micro-Doppler-Effect'' [9] is the key ability to enable radar sensors to use classification algorithms to separate walking pedestrians from other weak reflecting or slowly moving targets. The raw micro-Doppler detections of a walking pedestrian are shown in Figure 12.

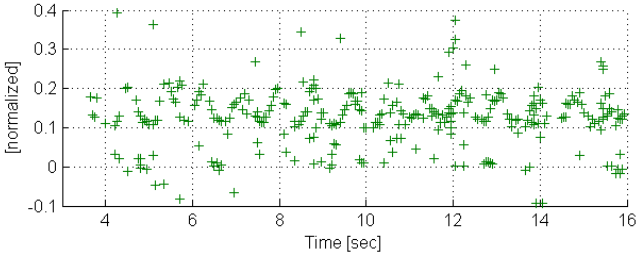

FIGURE 12. Normalized micro-Doppler detections of a walking pedestrian.

The micro-Doppler signature allows classifying pedestrians based on the following characteristics of their radar signals: Since all parts of a human body reflect radar signals (with different amplitudes) it is possible to detect the various limbs of the pedestrian. Hereby, the human walking movement is characterized by the typical periodical variations of the Doppler velocity. In contrast to that, rigid moving objects like cars have only one stable Doppler velocity according to the overall object velocity. Additionally, amplitudes are mainly low and the raw detections show a small regional extension. Before the classification of a walking pedestrian by common pattern classification algorithms, the raw detections have to be processed stepwise as shown in Figure 13. These steps can be summarized as the ''object detection'' of possible pedestrians.

In the preprocessing step, the raw detections from both sensors are transformed from the sensor polar coordinate system into the car-centered Cartesian coordinate system. Based on the precisely measured movement of the car the precisely measured Doppler is split into the Doppler which is induced by the movement of the car and the part which is

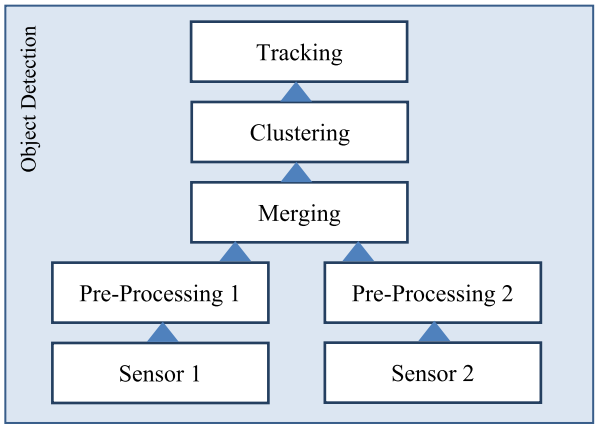

FIGURE 13. Object detection processing steps.

a result of the movement of the target. Thereafter, the detections are discriminated with regard to the following three types: stationary, slowly moving or fast moving. Using appropriate thresholds it is possible to identify slowly moving detections which could be caused by a pedestrian.

After all detections have been transformed to the coordination system of the car, it is possible to combine those from both frontal sensors by merging the two measurements with the minimal time difference to one set of frontal raw radar detections. In a next step, all detections which belong to the same object have to be identified by a clustering algorithm. The clustering, which is done by a modified DBSCAN algorithm, is focused on possible pedestrian targets by ignoring all fast moving detections and also all stationary detections which are too far away from the next slowly moving detection. These modifications are used to determine clusters containing all detections belonging to one possible pedestrian object, not only the slowly moving but also the near-stationary detections, which could belong to the leg in the standing phase. In the same processing step, immediately after the clustering, the average cluster values in position and velocity are calculated. These average cluster values are used in the next processing step to track the motion of the potential pedestrian using a Kalman filter over the consecutive measuring periods to determine the tracked object of the potential pedestrian object. Tracking is the final detection step and classification can take place. The classification process itself consists again of additional sub steps as shown in Figure 14.

In the first step of the classification process, the data of the tracked objects and the whole associated radar raw detection clusters are accumulated over some consecutive time steps. This step combines the raw information with the tracking data and increases the data basis for the following processing steps by accumulation over time. In the feature calculation step many different features are calculated based on the raw data, including micro-Doppler features, and also based on the tracking results such as the covariance matrix values. The normalization of these features is also performed here. In Figure 15 two features are exemplarily shown.

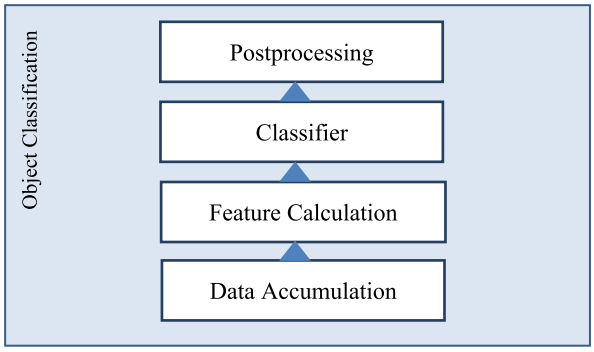

FIGURE 14. Pedestrian classification processing steps.

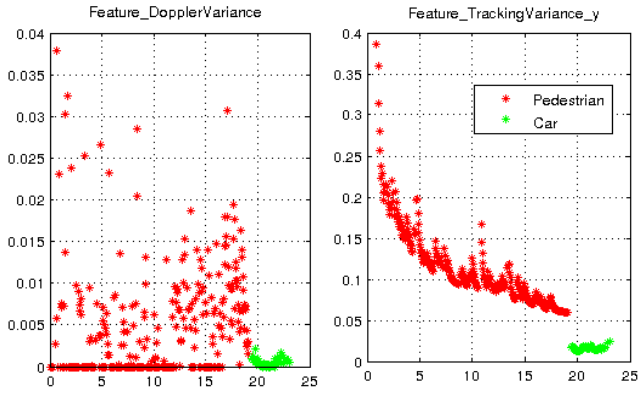

FIGURE 15. Examples: Pedestrian classification features.

The difference in these features between the walking pedestrian and the car, although it is just starting in this scene, is obvious. The Doppler Profile is calculated over all raw targets which belong to the cluster and the variance in y is directly provided by the Kalman Filter. All features, not only these two, were also normalized in the Feature Calculation step. Afterwards, these normalized features are evaluated by a neural-network classifier with one hidden layer. During training of the neural-network, a compromise between good classification results and over-fitting had to be found by adapting the number of hidden knots.

Finally, these raw classification values, which vary in part significantly from time step to time step, are stabilized. The variation is caused by different target densities of the pedestrian object. The stabilization is done in the post-processing step by a first threshold, which requires sequential high confidence values to identify a pedestrian for the first time, and afterwards by a second threshold, which evaluates a lower requirement to keep the positive identification as a pedestrian.

The result of this classification chain is a stable pedestrian classification, based on already available automotive radars sensors with a huge field-of-view and range in the area of interest in the front of the autonomous car combined with a high identification rate of walking pedestrians. This classification enables the car to identify pedestrians moving towards

a crosswalk early enough in all possible inner city scenarios to interact human-like with them and to respect the traffic rules autonomously.

V. RADAR BASED DRIVING LANE DETECTION AND REPRESENTATION

After processing the vehicles mobile and dynamic object list in a 360° environment, the next puzzle piece is to provide infrastructure like information. Among other information, an autonomous car like Bertha has to know the upcoming road course to stay on the road. To this end a camera is typically used to extract the lane markings. However, especially on rural roads lane markings are often hard to detect and environmental conditions like counter sun light or snow on the surface reduce the line markings detectability. Radar can help solve these issues. With the aid of imaging radar, the road course can be determined because the road surface deflects the radar signal away whereas the road boundary (e.g. guarding rails, grass, gravel, rough terrain) reflects the signal back towards the radar. The radar image of a rural road is shown in Figure 16 on the left.

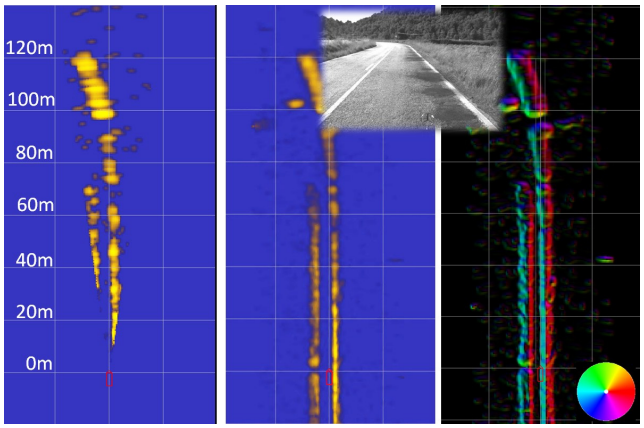

FIGURE 16. Left: original image. Middle: gridmap. Right: spatial derivative.

After applying a deconvolution of the image and building a grid map the road course becomes clearly visible (Figure 16 middle). The subsequent algorithm estimating the road course is based on the following assumptions:

- The road boundary is parallel to the road course
- The road surface is free of radar echoes

Mathematically this means two approximate constraints an appropriate road course has to fulfill are defined. These constraints are subsumed by a quality function introduced later on. The road course is estimated by maximizing the quality function over the parameters of the road model. The road model is introduced in the next section.

A. ROAD MODEL

Several road models are used in the literature. The most common one is a clothoid. This is driven by standards applied to road design. The third-order Taylor series expansion is used to get a computational feasible approximation of the clothoid. The vehicles ego-path therefore is a polynomial of third order:

$$y(x) = c_1 x + c_2 x^2 + c_3 x^3$$

where x is the longitudinal and y the lateral distance from the vehicle. The left and right borders of a road have different clothoid parameters depending on the lateral distances to the vehicle. They are calculated using the normal of the derivative at x, the lateral offset c_0 and the width w:

$$\begin{aligned}
\varphi(x) &= \operatorname{arccot}(c_1 + 2c_2 x + 3c_3 x^2) \\
x_{left}(x) &= x + cos(\varphi(x)) \cdot c_0 \\
y_{left}(x) &= y(x) + \sin(\varphi(x)) \cdot c_0 \\
x_{right}(x) &= x + cos(\varphi(x)) \cdot (c_0 - w) \\
y_{right}(x) &= y(x) + \sin(\varphi(x)) \cdot (c_0 - w)
\end{aligned}$$

The angle $\varphi(x)$ is orthogonal to the derivative of $y(x)$. The vehicle is in-between the left and right border if w is greater than c_0 and both are greater than 0. Figure 17 illustrates how the left and right borders are calculated.

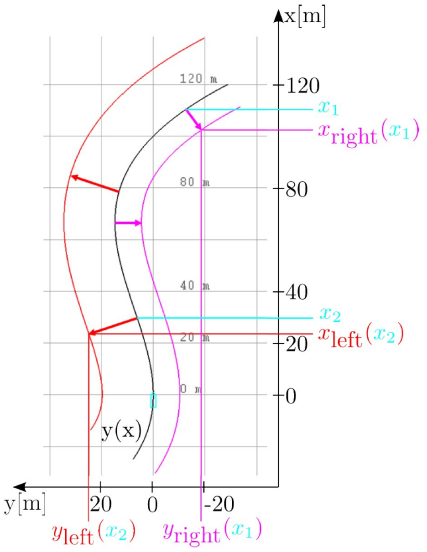

FIGURE 17. Road model; the left border is plotted in red and the right one in magenta. The black lane is the road course. x_1 and x_2 show the calculation of the right and left border, respectively.

B. QUALITY FUNCTION

The quality function is based on the following assumptions:

- The angle of the spatial derivative at the road boundary is orthogonal to the road course.
- The amplitude of the spatial derivative reaches its maximum at the road boundary.
- The amplitude of the grid map is zero on the road surface.

The first two assumptions lead to the first part of the quality function:

$$D(S) = \frac{\sum_{\vec{p} \in S} \left[A(\vec{p}) \cdot (1 - |\varphi_I(\vec{p}) - \varphi_M(\vec{p})| \right]}{|S|}$$

with S the set of all pixels on the road boundary, $\vec{p} = (x, y)$ a point on the grid map, $A(\vec{p}) \in [0, 1]$ the amplitude of the gridmap, $\varphi_I(\vec{p})$ the angle of the spatial derivative and $\varphi_M(\vec{p})$ the angle of a given road course.

$D(S)$ measures the weighted sum of angle deviations along a given road course. The higher $D(S)$ is, the more the road model is parallel to the measured radar data.

The second part of the quality function, namely $R(S)$, measures the weighted sum of reflections on the road surface:

$$R(S) = \frac{\sum_{\vec{p} \in C(S)} A(\vec{p})}{|C|}$$

with $C(S)$ the set of all pixels of the gridmap inside the road boundary. The overall quality function $Q(S)$ then is:

$$Q(S) = D(S) - R(S)$$

S contains all pixels (x, y) on the boundary of a given road course and is defined by:

$$S = \left\{ (x, y) \left| \begin{array}{l} ((x = x_{left}(x_0) \cap y = y_{left}(x_0)) \cup \\ ((x = x_{right}(x_0) \cap y = y_{right}(x_0)) \end{array} \right. \right\}$$

with $x_0 \in [0m, 120m]$.

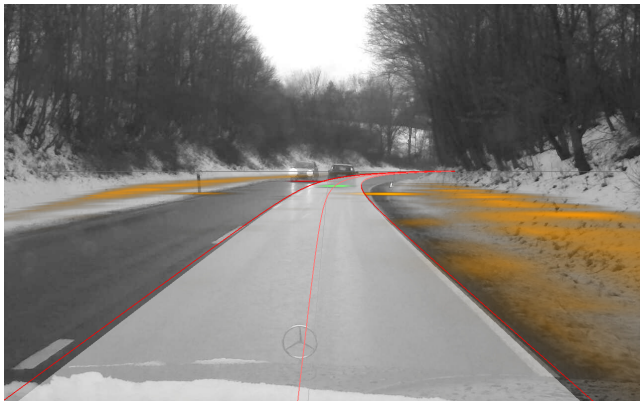

FIGURE 18. Estimated road course mapped onto the image of the monitoring camera.

C. MAXIMIZING THE QUALITY FUNCTION

The road course is eventually found by maximizing $Q(S)$ over the road model parameters: c_0, c_1, c_2, c_3. Figure 18 shows the result. For more details the reader is referred to [20].

The next important step is to provide the static object information to the vehicle. This will allow a more comprehensive understanding of the situation if the dynamic world will be combined with infrastructure and the static environment. This step is described in the following section.

VI. RADAR-GRIDS FOR REPRESENTING THE STATIONARY ENVIRONMENT

The goal of this step is to compute an occupancy grid as introduced by Elfes [10] in order to accumulate the radar data of all stationary detections over time. The occupancy grid map $M_k = \{m_1, m_2, \ldots, m_N\}$ consists of N grid cells m_i, which represent the environment as a 2D-space with equally sized cells. For the current localization and obstacle detection application, the grid cell size is fixed to 0.1m $\times$ 0.1m. Each cell is a probabilistic variable describing the occupancy of this cell. Assuming that M_k is the grid map at time k and that the grid cells are independent one to another, the occupancy grid map can be modeled as a posterior probability:

$$P(M_k | Z_{1:k}, X_{1:k}) = \prod_i P(m_i | Z_{1:k}, X_{1:k})$$

where $P(m_i | Z_{1:k}, X_{1:k})$ is the inverse sensor model, which describes the probability of occupancy of the ith cell, given the measurements $Z_{1:k}$ and the dynamic object state $X_{1:k}$.

Each measurement consists of n radar detections $Z_j = \{z_{\{1,j\}}, z_{\{2,j\}}, \ldots, z_{\{n,j\}}\}$.

The occupancy value of each cell is calculated by a binary Bayesian filter. In practice, the log posterior is used to integrate new measurements efficiently. Instead of performing multiplications, using the log odds ratio simplifies the calculation to addition and avoids instabilities of calculating probabilities near zero or one. The log odds occupancy grid map is formalized as:

$$L_k(m_i) = log \frac{P(m_i | Z_{1:k}, X_{1:k})}{1 - P(m_i | Z_{1:k}, X_{1:k})}$$

The recursive formulation of map update in log odds ratio form is given by [11]:

$$L_k(m_i) = L_{k-1}(m_i) + log \frac{P(m_i | Z_{1:k}, X_{1:k})}{1 - P(m_i | Z_{1:k}, X_{1:k})} - L_0(m_i)$$

where $L_{k-1}(m_i)$ and $L_0(m_i)$ are the previous and prior log odds values of grid cell i. Assuming that no prior knowledge is available, the prior probability of unknown cells is set to $P(m_i) = 0.5$, the above equation produces the prior log odds ratio $L_0 = 0$. The log odds formulation of the above equation can be inverted to obtain the corresponding probability of map M_k. A radar based occupancy map is displayed in Fig 19. The map is projected into the image of the documentation camera so that one can appreciate how the radars perceive the environment.

A. OBJECT DETECTION

Object detection and scene understanding are key components in Advanced Driver Assistance Systems. In order to enable autonomous driving in semi-structured environments low level mapping must be further processed to achieve a high level of awareness [12].

A result of for the real-time algorithm [13] capable of detecting both parallel and cross-parked vehicles from radar data is depicted in Fig. 20. Parked vehicle candidates are then extracted from the occupancy grid representing the stationary environment. These candidates are described and classified in order to assert the presence of vehicles. The proposed method addresses the challenge of detecting both parallel and cross-parked vehicles. A distinction is made between cross-parked vehicles, which stand perpendicular to the lane direction, and

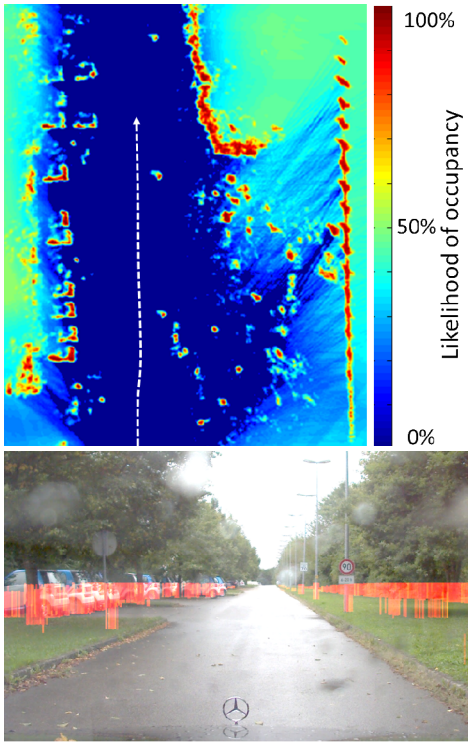

FIGURE 19. Radar occupancy grid (top) and its projection into the documentation camera image (bottom). The map colors represent the probabilities of occupancy. The driven path is plotted as dashed white line.

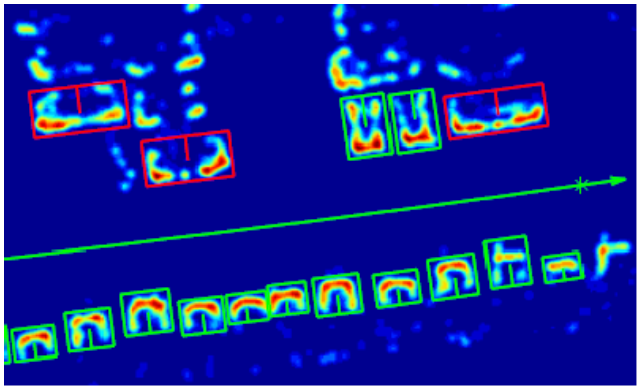

FIGURE 20. Parked vehicle detection in a parking lot. Vehicle trajectory is represented by a green line. Red and green boxes respectively represent parallel-parked and cross-parked vehicles which are detected by the system. It is interesting to note that the classifiers correctly distinguished the two cross-parked SMART vehicles from the larger parallel-parked vehicle at the top right.

parallel-parked vehicle, which are obviously parallel to the lane direction.

Radar data has been recorded during different sequences ranging from a drive in a parking crowded with perpendicular parked vehicles to a drive on an urban street with dispersed parallel-parked vehicles. From these data, lists of candidate have been pre-processed and carefully labeled. As a result, two data sets were created. The perpendicular-parked

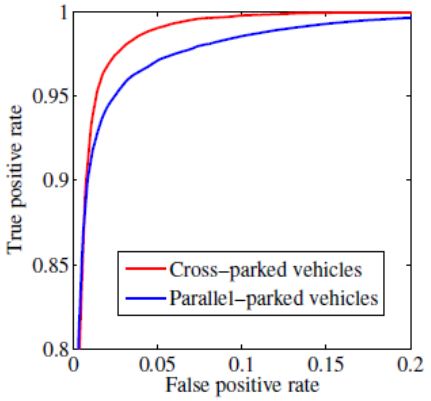

FIGURE 21. Average ROC curves for cross-parked and parallel-parked vehicles classification.

vehicles set contains 1119 samples (268 true vehicles and 851 false vehicles) while the parallel-parked vehicles set contains 1342 samples (300 true vehicles and 1042 false vehicles). In order to predict the performance of the classifiers, a repeated random sub-sampling validation was performed. As depicted in Fig. 21 the average accuracy of the classifiers is 97.9% $\pm$ 0.7% for perpendicular-parked vehicles and 96.9% $\pm$ 0.7% for parallel-parked vehicles.

VII. KEY PERFORMANCE FACTOR: PACKAGING OF MMW RADARS

Purely based research results of environmental sensors typically do not consider packaging issues. This becomes quite obvious while inspecting the vehicles used in the DARPA grand challenge or other autonomous vehicle projects [4]. However, one key performance factor for managing the transfer from research to serial implementation is how to package environmental sensors in standard vehicles like sedans. One big advantage of automotive radars from the vehicle design point of view is their capability to be mounted invisibly behind painted bumpers or other layered structures. Any of these radar sensor covers has to be designed carefully to avoid performance degradation due to transmission losses, reflections, and edge effects.

Even more than for lower operating frequencies, this is a crucial issue concerning sensor systems working in the frequency range from 76 GHz to 81 GHz. Bumpers and other components mounted on a vehicle's front- or rear-end have to be considered as radome structures. Unlike for lower frequencies e.g. used for UWB radar or communication, in the desired frequency range, the material thickness is not electrically thin and thus much smaller than the wavelength. Strong reflection back to the sensor and high transmission loss will cause performance degradation of the radar sensor. This chapter will focus on the challenging needs and trade-offs connected with hidden radar sensor integration in automotive platforms.

The base vehicle of the Bertha Benz research car was a series-production Mercedes Benz S class. One important goal

of the project was to demonstrate the fully autonomous long distance drive with state-of-the-art radar sensors and cameras with sensor integration as close to the series production's conditions as possible. Therefore, exterior parts such as e.g. bumpers were not modified substantially.

As with every other automotive sensor development project, the integration of extra sensors at new mounting positions had to be carefully prepared. Several of the issues lead to conflicting requirements. In effect, radar sensor integration is a highly complex system engineering task.

There are several issues directly linked to the electromagnetic behavior of multi-layer structures, with the RF MMICs (radio frequency monolithic microwave integrated circuit) in the sensors and radar signal processing results:

- electromagnetic characteristics of exterior material and paint (permittivity and loss tangent)
- tolerance of the sensor against direct reflection between exterior parts and the sensor
- vehicle design and shape of parts covering the sensor
- tolerance of the sensor against angular distortion due to transmission through exterior parts
- manufacturing tolerances (variation of paint and exterior material thickness as well as variation of material composition)
- multiple paint layers, especially repairs
- coverage of exterior parts with water, snow, ice, dust or salt, etc.
- functional demands for field of view, detection range and sensitivity of the radar sensor

Furthermore, there are several influences and requirements of other engineering divisions that have to be considered:

- mechanical stability of exterior parts and assembly group in crash scenarios
- mechanical tolerance and variation of position and angle of the sensor relative to car body shell, mounting bracket or exterior part
- cooling air blockage to be minimized by the presence of a front radar
- power dissipation of the sensor and probably high ambient temperature close to engine and exhaust system
- installation space conflicts with other components

During the past years, extensive studies of manufacturing tolerances and the composition of substrate materials as well as paint were carried out by Daimler AG (see [14]–[16]). Those results were the foundation of the sensor integration in the Bertha Benz vehicle.

An electromagnetic wave traveling from air through a dielectric medium and back to air is reflected partially at both boundary layers. Modelling the scattering parameters (also known as S parameters) lead to a useful characterization of the electromagnetic behavior of the transition between different materials [17].

One possible way to analytically describe material transitions is depicted in Fig. 22. The electric field E of an electromagnetic wave at a dedicated point of time is

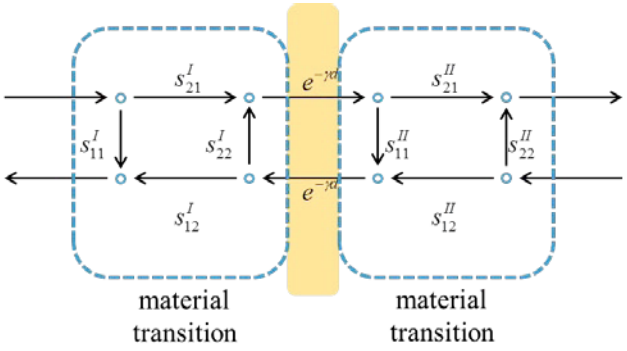

FIGURE 22. Transition between air and a dielectric medium of thickness d. S parameters represent the portions of an electromagnetic wave that are transmitted and reflected at the dielectric boundaries.

given by

$$E = E_0 e^{-jkz}$$

where k is the wave number depending on the frequency of the wave, z is its direction of propagation and E_0 is its amplitude. The wave impedance Z related to the propagation in an isotropic dielectric medium is

$$Z = \sqrt{\frac{\mu_0 \mu_r}{\varepsilon}} = \frac{120\pi\,\Omega}{\sqrt{1 - j\tan\delta}}$$

with the impedance of free space $Z_0 = 120\pi\,\Omega$, the magnetic constant μ_0, and the parameter defining the material's electromagnetic properties: permeability μ_r, complex permittivity ε and the electric loss tangent $\tan\delta$.

At the boundary between air and dielectric medium, the wave is split into a transmitted and a reflected wave. The relationship between incoming wave and those portions is given by the S parameters s_{11}^{I} for reflection and s_{21}^{I} for transmission

$$s_{11}^{I} = -s_{22}^{I} = -s_{11}^{II} = s_{22}^{II} = \frac{Z_{air} - Z_{medium}}{Z_{air} + Z_{medium}} \quad \text{and}$$

$$s_{21}^{I} = s_{12}^{I} = s_{21}^{II} = s_{12}^{II} = \frac{\sqrt{2 Z_{air} \cdot Z_{medium}}}{Z_{air} + Z_{medium}}.$$

The propagation through the dielectric medium with its thickness d is given by the multiplicator $e^{-j\gamma d}$, where

$$\gamma = jk = jk_0 \frac{\varepsilon}{\varepsilon_0}$$

is the complex propagation constant with the wave number

$$k = \frac{2\pi}{\lambda}.$$

From the S parameters given above, terms for reflection amplitude $|r|$ and transmission amplitude $|t|$ of the electromagnetic wave can be calculated. The representation of material transitions with S parameters is not only possible for single layer materials, but also for stacks of arbitrary homogenous and isotropic materials.

Depending on the frequency of the wave and the thickness and material properties of the dielectric medium, the reflected

and transmitted portions of the wave show constructive or destructive interference. For a certain multi-layer material setup, one can derive a local optimum of the thickness of the dielectric medium. This reduces reflection of the electromagnetic wave back to the sensor and transmission through the exterior part. The effects can be investigated with the help of antenna measurements, full wave simulations or analytical investigations.

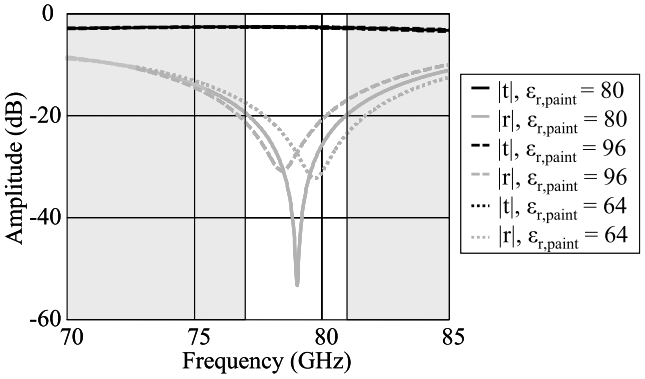

FIGURE 23. Simulation of transmission $|t|$ and reflection $|r|$ through a bumper with metallic paint. Variation of the permittivity of the paint $\varepsilon_{r,paint}$ shifts the reflection minimum.

As an exemplary result of analytical investigations, Fig. 23 shows the transmission $|t|$ and the reflection $|r|$ through a bumper with metallic paint. The simulation was carried out with a multi-layer model implemented in Matlab. For the ideal case of properly chosen bumper thickness (in this example 3.44 mm), the result is a reflection $|r|$ better than -20 dB for the whole frequency band from 77 to 81 GHz. Introducing a variation of the material characteristics of the paint would shift the desired minimum of $|r|$ to lower or higher frequencies. In this case, the permittivity is changed. Nevertheless, the transmission $|t|$ stays approximately constant.

There are several ways to optimize a radome for the needs of hidden radar sensor integration. Considering manufacturing tolerances, varying material combinations and required bandwidth, thickness optimization of the substrate material was found to be a good compromise between RF performance, costs and effort [14]. Other approaches are quarter wavelength transforming structures, FSS structures (frequency selective surface) or inductive structures on the back side of the radome (e.g. in [16]). Thickness optimization by applying layers of special adhesive foil was found to be the most suitable for the Bertha Benz research car. This way, the standard bumpers could be adapted for radar sensors operating in the 77 GHz frequency range.

VIII. FREQUENCY MANAGEMENT: PAVING THE GROUND FOR WORLDWIDE USE OF RADARS

Generally, frequency management and interference studies are very often underrepresented in research reports and development projects. However, at the end they are the final gate to market introduction. Interoperability is a key issue especially the more the market penetration with radar sensors develops. Frequency management is mandatory for frequency regulation, the imperative permission status before market introduction. Chapter VIII provides a brief overview on the status of both radar development activities.

During the last years, much progress has been made in the frequency regulation for automotive radar. The 76–77 GHz ACC band was regulated in the 1990's already, followed by standardization in Europe. Now this band is allocated for Intelligent Transport Services in many countries. Some harmonization efforts still have to be carried out, e.g., closing of a frequency gap in Japan.

For short range applications beneath ISM narrowband systems at 24-24.05 GHz, UWB sensors (bandwidth $>$ 500 MHz) are widely applied, because of their possible real-time high-range resolution. The Federal Communications Commission (FCC) regulated UWB for the North American market in 2002 already. For automotive UWB short range radar systems the FCC allocated the 22–29 GHz band, with a maximum mean power density of -41.3 dBm/MHz.

In 2002, more than 30 mainly European car manufacturers and suppliers founded the Short range Automotive Radar frequency Allocation consortium (SARA). SARA's main objective was to support UWB regulation for automotive radar in the 24 GHz range in Europe. Because of strong objections by the telecom industry and earth observation institutions, a lot of effort was dedicated to find a compromise and to enable automotive UWB radar systems. In 2012, the successor of SARA, the Global Automotive Radio Regulations Group (GARREG) was founded in order to promote the interests of the global automotive industry.

On 17 January 2005 the commission of the European Community EC finally allocated the range of 21.65–26.65 GHz for UWB short range radar. The marketing of these systems in Europe is allowed till 2018. Hence, in March 2004 the European commission allocated the 77–81GHz frequency range for UWB SRR with permitted usage from 2005 onwards. This band has been identified in ITU as the definitive band for automotive SRR (ITU-R M1452). The worldwide establishment and speed up of the harmonized 79 GHz frequency allocation is carried out intensively under the frame of the EC funded "79 GHz"-project [18]. In the interim phase, automotive OEMs integrate mid- and short range sensors operating in the 76-77 GHz band.

During the next decade, a frequency shift to frequencies above 100 GHz seems probable, in particular due to further reduction of the RF frontend aperture size. At 122 GHz, an ISM band is available with an allocated bandwidth of 1 GHz. Unfortunately, this does not fulfil the announced minimal bandwidth requirement of 2 GHz. With respect to design considerations of future sensors, frequencies around 150-160 GHz are under discussion (twice the present operational frequencies). At present, there is no allocation available in this band for automotive radar operation.

Recently, the interest of non-automotive applications to use the mature and cost efficient automotive radar technology has been observed (e.g. SAR helicopter landing support, airplane wingtip sensors, road monitoring, level gauging ...). This requires a sophisticated evaluation of the criticality of these applications with respect to automotive functions, in particular safety and autonomous applications and their protection needs.

Beneath the discussed spectrum engineering and frequency management issue, dealing with enabling coexistence between automotive radar and other services, electromagnetic compatibility are of crucial importance for automotive radar operation.

Automotive radars have to avoid interference of automotive radars operated in other cars and have to be resistant against interference of these external radars. This can be solved by technical as well as standardization measures. Extensive studies on sensor-sensor interference and -mitigation have been conducted within the EC FP7 public funded MOSARIM project [19]. In MOSARIM a set of design rules and design guidelines has been developed. These guidelines form the basis for the design and development of future interoperable automotive radar sensors.

IX. SUMMARY

Bertha successfully drove approximately 100 km of the Bertha Benz Memorial Route in public traffic fully autonomously. For the environmental perception, eight Radar sensors have formed the 360° environmental perception backbone assisted by a front-looking stereo camera. This paper presents performance results which have never been envisioned for automotive radars before. Accompanying the development of an appropriate packaging process, the foundation has been laid for application of the research activities to series production. With Bertha, radar has started it's metamorphosis from a simple detector to an imaging-like device: A Radar-Eye. This is a research trend that has to be continued to make an autonomous-driving product a reality.

Beside the necessary further evolution of technology topics the realization of fully autonomous vehicles of course faces a lot more challenges.

Legislation, liability and regulation issues have to be solved on a common basis and as a key factor the public trust and acceptance in this new technology has to be achieved. Most of these topics are meanwhile at least initially addressed and first intermediate steps towards the final vision of fully autonomous vehicles are currently on its way.

REFERENCES

[1] J. Ziegler *et al.*, "Making Bertha drive—An autonomous journey on a historic route," *IEEE Intell. Transp. Syst. Mag.*, vol. 6, no. 2, pp. 8–20, Summer 2014.
[2] U. Franke *et al.*, "Making Bertha see," in *Proc. IEEE ICCV Workshop*, Sydney, NSW, Australia, Dec. 2013, pp. 214–221.
[3] J. Dickmann, N. Appenrodt, and C. Brenk, "Making Bertha," *IEEE Spectr.*, vol. 51, no. 8, pp. 44–49, Aug. 2014.
[4] M. Buehler, K. Iagnemma, and S. Singh, Eds., *The DARPA Urban Challenge* (Springer Tracts in Advanced Robotics), vol. 56. Berlin, Germany: Springer-Verlag, 2009.
[5] Y. Bar-Shalom, "Update with out-of-sequence measurements in tracking: Exact solution," *IEEE Trans. Aerosp. Electron. Syst.*, vol. 38, no. 3, pp. 769–777, Jul. 2002.
[6] M. M. Muntzinger *et al.*, "Reliable automotive pre-crash system with out-of-sequence measurement processing," in *Proc. IEEE Intell. Vehicles Symp.*, Jun. 2010, pp. 1022–1027.
[7] M. M. Muntzinger, F. Schröder, S. Zuther, and K. Dietmayer, "Out-of-sequence measurement processing for an automotive pre-crash application," in *Proc. 12th IEEE Int. Conf. Intell. Transp. Syst.*, Oct. 2009, pp. 1–6.
[8] M. Ester, H.-P. Kriegel, J. Sander, and X. Xu, "A density-based algorithm for discovering clusters in large spatial databases with noise," in *Proc. 2nd Int. Conf. Knowl. Discovery Data Mining (KDD)*, 1996, pp. 226–231.
[9] V. Chen, *The Micro-Doppler Effect in Radar*. Norwood, MA, USA: Artech House, 2011, pp. 157–193.
[10] A. Elfes, "Using occupancy grids for mobile robot perception and navigation," *Computer*, vol. 22, no. 6, pp. 46–57, Jun. 1989.
[11] S. Thrun, W. Burgard, and D. Fox, *Probabilistic Robotics*, vol. 1. Cambridge, MA, USA: MIT Press, 2005.
[12] D. Dolgov and S. Thrun, "Autonomous driving in semi-structured environments: Mapping and planning," in *Proc. IEEE Int. Conf. Robot. Autom. (ICRA)*, May 2009, pp. 3407–3414.
[13] R. Dubé, M. Hahn, M. Schütz, J. Dickmann, and D. Gingras, "Detection of parked vehicles from a radar based occupancy grid," in *Proc. IEEE Intell. Vehicles Symp.*, Jun. 2014, pp. 1415–1420.
[14] H. L. Bloecher, C. Fischer, and A. Sailer, "Prerequisites of mmW automotive radar specification, platform integration and operation," in *Proc. Eur. Radar Conf. (EuRAD)*, Oct. 2013, pp. 192–195.
[15] F. Fitzek, R. H. Raßhofer, and E. M. Biebl, "Broadband matching of high-permittivity coatings with frequency selective surfaces," in *Proc. German Microw. Conf. (GeMIC)*, Mar. 2011, pp. 1–4.
[16] A. Sailer, "Verdeckte Integration von Radarsensoren im automobilen Umfeld," presented at the VDE ITG-Workshop Automotive Antennen, Munich, Germany, Sep. 2012.
[17] D. J. Kozakoff, *Analysis of Radome-Enclosed Antennas*. Norwood, MA, USA: Artech House, 1997.
[18] *Including Informations on Automotive Radar Frequency Allocation*. [Online]. Available: http://www.79ghz.eu, accessed Nov. 2014.
[19] [Online]. Available: http://www.mosarim.eu, accessed Nov. 2014.
[20] F. Sarholz, J. Mehnert, J. Klappstein, J. Dickmann, and B. Radig, "Evaluation of different approaches for road course estimation using imaging radar," in *Proc. IEEE/RSJ Int. Conf. Intell. Robots Syst.*, San Francisco, CA, USA, Sep. 2011, pp. 4587–4592.

JUERGEN DICKMANN received the Diploma degree in electrical engineering from University Duisburg, Germany, in 1984, and the Dr.Ing. degree from RWTH Aachen University, Germany, in 1991. In 1986, he was with the AEG Research Center, researching III/V processing techniques, millimeter-wave devices, and monolithic microwave integrated circuits. Since 1990, he has been with the Group Research and Advanced Engineering, Daimler AG, where he is currently responsible for active sensors.

NILS APPENRODT received the Dipl.-Ing. degree in electrical engineering from University Duisburg, Germany, in 1996. He was a Research Assistant in the field of imaging radar systems with University Duisburg, where he was involved in close cooperation with the Daimler Research Institute, Ulm, Germany. Since 2000, he has been with the Group Research and Advanced Engineering, Daimler AG, as a Research Engineer and the Manager, where he is mainly working in the field of environment perception systems. His research interests include radar and laser sensor processing, sensor data fusion, and safety systems.

JENS KLAPPSTEIN received the Diploma degree in computer science from the Technical University of Ilmenau, Germany, in 2004, and the Dr.rer.nat. degree from the University of Heidelberg, Germany, in 2008. Since 2004, he has been with the Group Research and Advanced Engineering, Daimler AG, where he is currently a Research Engineer. His research interests comprise signal processing of radar images and high-resolution algorithms.

HANS-LUDWIG BLOECHER received the Dipl.-Ing. (M.Sc.) degree in communications engineering and the Dr.Ing. (Ph.D.) degree in microwave, radar, and antenna engineering from the University of Siegen, Germany, in 1990 and 1997, respectively. In 1997, he joined Daimler-Benz Aerospace (now AIRBUS D&S) as a Radar Systems Engineer and Technical Project Leader, working on ground/naval radars and multispectral missile seekers. Since 2001, he has been with the Group Research and Advanced Engineering, Daimler AG, where he is currently a Principal Researcher and the Project Manager in the active sensors branch. Since 2004, he has been the Project Leader of Daimler's activities of the BMBF and EU public funded projects dealing with 77/79 GHz next-generation automotive radar. Since 2001, he represents Daimler AG in international spectrum engineering and standardization gremia.

MARC MUNTZINGER received the Diploma degree in electrical engineering from Technical University Munich, Germany, in 2006, and the Dr.Ing. degree from the Institute of Measurement, Control, and Microtechnology, Ulm University, Germany, in 2011. Since 2006, he has been with the Group Research and Advanced Engineering, Daimler AG, where he was a Research Engineer. Since 2014, he has been with Porsche AG. His research interests comprise multitarget tracking, advances in radar technology, and highly automated driving.

ALFONS SAILER received the Dipl.-Ing. degree in electrical engineering from Ulm University, Germany, in 2008. From 2008 to 2012, he was a Research Assistant with the Institute of Microwave Techniques, Ulm University. Since 2012, he has been with the Group Research and Advanced Engineering, Daimler AG, where he is currently a Research Engineer. His research interests include antenna and radar technology, sensor concepts for future driver assistance systems, and vehicle integration of active sensors.

MARKUS HAHN received the Diploma degree in computer science from the Technical University of Ilmenau, Germany, in 2007, and the Ph.D. (Dr.Ing.) degree in computer science from the University of Bielefeld, in 2011. Since 2012, he has been a Senior Research Scientist with the Daimler Research Centre Ulm. His fields of research are signal and image understanding, radar technology, mobile robotics, and the applications of pattern understanding methods to real-world scenarios of automotive driving.

CARSTEN BRENK received the Dipl.-Ing. (FH) degree in mechanical engineering from the University of Applied Sciences Bonn-Rhein-Sieg, Germany, in 2007, and the Dipl.-Kfm. degree in business economics from Correspondence University Hagen, Germany, in 2010. Since 2007, he has been with the Group Research and Advanced Engineering, Daimler AG, where he is currently a Research Engineer. His research interests comprise mirco-Doppler radar signals and object classification algorithms.